Small Matrix Path Integral for System-Bath Dynamics

Nancy Makri*

Departments of Chemistry and Physics, University of Illinois,
505 S. Mathews Avenue, Urbana, Illinois 61801

Abstract

A small matrix decomposition of the path integral expression (SMatPI) that yields the reduced density matrix of a system interacting with a dissipative harmonic bath is obtained by recursively spreading the entangled influence functional terms over longer time intervals, while simultaneously decreasing their magnitude, until these terms become negligible. This allows summing over the path integral variables one by one through multiplication of small matrices with dimension equal to that of the bare system. The theoretical framework of the decomposition is described using a diagrammatic approach. Analytical and numerical calculations show that the necessary time length for the temporal entanglement to become negligible is practically the same as the bath-induced memory. The properties and structure of the propagator matrices are discussed, and applications to multistate systems are presented.

*Email: nmakri@illinois.edu

I. Introduction

In spite of persistent efforts, solving without assumptions the quantum mechanical equations that govern the time evolution of physical observables in systems of many degrees of freedom remains a formidable task. Among wavefunction-based approaches, the multiconfiguration time-dependent Hartree (MCTDH) method[1] has shown impressive capabilities for molecular systems, and the density matrix renormalization group (DMRG) approach[2] can successfully treat extended systems of a one-dimensional topology. Nevertheless, methods based on wavefunctions are not naturally suited to condensed phase processes, where hundreds or thousands of molecular vibrations and/or phonons need to be treated at finite temperature, as the relevant Hilbert space is far too large. Further, combining wavefunction-based methods with classical trajectories involves uncontrolled approximations. A number of density matrix approaches have been investigated, which involve master equations (with or without perturbative or Markovian assumptions) and stochastic Schrödinger equation treatments.

Feynman's path integral formulation,[3, 4] which does not require wavefunction storage, offers a very attractive starting point which is ideally suited to the calculation of a system's reduced density matrix (RDM). Harmonic bath degrees of freedom (e.g. any number of phonons or normal mode vibrations), which are responsible for dissipative dynamics,[5-7] can be integrated out analytically, at zero or finite temperature, giving rise to the well-known Feynman-Vernon influence functional.[8] Many complex systems can be realistically treated only in combination with classical trajectory treatments, but the incompatibility of Schrödinger's and Newton's formulations necessitates major assumptions.[9] However, because quantum paths are spatially local, their interaction with classical trajectories is straightforward and unambiguous within Feynman's framework. The quantum-classical path integral[10-12] (QCPI) offers a rigorous approach that treats the interaction of a quantum system with its environment correctly and in full atomistic detail.[13]

The main practical issue with path integral methods is the introduction of two auxiliary variables per time step for each quantum degree of freedom, leading to exponential proliferation of the number of terms with the propagation time. Monte Carlo methods[14] generally fail to converge when applied to the real-time path integral because of a sign problem associated with the quantum mechanical phase. Since the early 1990s, a number of algorithms have emerged that enable numerically exact evaluation of the path integral for systems coupled to harmonic environments.[15-32] In particular, exploiting the finite length of nonlocal 'memory' interactions in the influence functional allows iterative evaluation of the path integral,[17, 18] which leads to linear scaling with the number of propagation steps.

Fully quantum mechanical real-time path integral methods are not necessarily restricted to harmonic baths. Iterative decompositions (which allow linear scaling with propagation time) have been extended to fermionic baths,[33, 34] and have been shown to be generalizable to arbitrary environments,[35] as long as the influence functional is available (analytically or numerically). Further, a modular decomposition of the path integral[36, 37] (MPI) allows treatment of the dynamics in extended systems with a quasi-one-dimensional topology, where hundreds of vibrational coordinates that couple to the electronic states of each unit can be treated without a significant increase in computational cost.

Nevertheless, the main limitation of iterative path integral algorithms (even in the ideal case of a harmonic bath) continues to be their rather steep scaling with the number n of system states. In general, one needs to construct and store an array which contains all relevant quantum mechanical paths that span the memory length $\Delta k_{\max}\Delta t$, where the parameter $\Delta k_{\max}$ is the number of path integral time steps Δt that span the bath-induced memory. Since the paths have forward and backward components, they form an

array of $n^{2\Delta k_{\max}}$ elements, and propagation involves $n^{2\Delta k_{\max}+2}$ operations per iteration step.[38] Because the influence functional fully couples the path variables at all time points within the memory length, the resulting structure is fully entangled and thus cannot be factored any further. Fortunately, filtering techniques[19-22] and singular matrix contraction[32] can dramatically reduce these numbers (and in many cases significantly slow down the exponential scaling). In the incoherent (high temperature and strong coupling to sluggish baths) regime, the blip decomposition[28, 29] offers exponential acceleration of the path sum by exploiting blip density as a powerful filtering criterion and (most importantly) by decreasing the number of stored path configurations from $n^{2\Delta k_{\max}}$ to n^{2b}, where b is the number of blips (i.e. non-identical forward-backward path regions) within the memory length. While these acceleration techniques can lead to very substantial savings, it is clear that the availability of rigorous path integral methods which do not require the storage of large path arrays would expand the applicability of real-time path integral methods to multistate systems.

A recent Communication[39] showed that it is possible to disentangle the path integral even within the memory length, by recursively shifting the entangled terms to longer time intervals while reducing their magnitude, until these terms become negligible. This variable decoupling leads to a small matrix decomposition of the path integral (SMatPI), where the relevant propagator matrices have dimensions equal to that of the system's RDM. Each of these matrices contains all the entangled influence functional interactions up to a particular time length that in practice does not exceed the bath-induced memory, and is obtained through a non-iterative path integral calculation. Once the SMatPI matrices have been computed, propagation to long times is extremely efficient. If full path sum calculations are employed, the SMatPI matrices require the evaluation of $n^{2\Delta k_{\max}}$ terms, but as explained earlier filtering techniques can dramatically decrease this effort. Because the SMatPI algorithm requires no array storage besides that of a few small matrices, it is realistically applicable to multistate systems. Most importantly, the SMatPI decomposition involves a systematic procedure similar to the iterative decomposition (which relies on decreasing memory), which does not involve any approximations or assumptions, and which converges to the full path integral result.

The present paper fully develops the SMatPI decomposition, using a diagrammatic approach to illustrate the entanglement of the path integral variables and motivate its recursive removal, and discusses the structure of the SMatPI matrices and the behavior of the entangled 'remainder' term. The description begins in section II with the necessary background on the path integral expression and the composition of the influence functional. Section III develops the decomposition, using the simplest case of two-step memory to illustrate in detail the procedure algebraically, as well as in terms of a diagrammatic representation of the discretized influence functional. Section IV discusses the entanglement length and its relation to the memory length using the zero-temperature spin-boson model as an analytical example, and also through numerical calculations. The properties and structure of the SMatPI matrices are discussed in section V. Applications of the algorithm on a dissipative two-level system in an interesting regime, as well as on an 11-state Hückel-type model (with and without next-nearest-neighbor couplings) are presented in section VI, and some concluding remarks are given in section VII.

II. Path integral and influence functional

The Hamiltonian describing a system interacting with dissipative harmonic bath has the form

$$\hat{H} = \hat{H}_{\rm sys} + \sum_j \left(\frac{\hat{p}_j^2}{2m_j} + \frac{1}{2} m_j \omega_j^2 \hat{x}_j^2 - c_j \hat{s} \hat{x}_j \right). \tag{2.1}$$

Here the Hamiltonian $H_{\rm sys}$ describes a discrete system of n states, or a continuous system which has been discretized via a discrete variable representation (DVR) of the path integral.[16] In either case, the system Hamiltonian, and also the coordinate operator $\hat{s}$, are given by $n \times n$ matrices,

$$\hat{H}_{\rm sys} = \sum_{i=1}^{n} \sum_{j=1}^{n} |\sigma_i\rangle h_{ij} \langle \sigma_j|, \quad \hat{s} = \sum_{i=1}^{n} |\sigma_i\rangle \sigma_i \langle \sigma_i|, \tag{2.2}$$

and $\{x_j, p_j\}$ denote the coordinate and momentum variables of the bath degrees of freedom. The focus is on observables pertaining to the system, which may be obtained from the RDM. It is commonly assumed that the initial RDM is a product of system and bath components, $\rho(0) = \rho_{\rm sys}(0)\rho_{\rm b}(0)$.

Consider the reduced propagator (RP) of the system at the time $N\Delta t$ (where Δt is the path integral time step), which is defined as the matrix $\mathbf{U}^{(N0)}$ with elements

$$U^{(N0)}_{i_N^\pm i_0^\pm} = {\rm Tr}_{\rm b} \left\langle \sigma_{i_N^+} \left| e^{-i\hat{H}N\Delta t/\hbar} \right| \sigma_{i_0^+} \right\rangle \hat{\rho}_{\rm b}(0) \left\langle \sigma_{i_0^-} \left| e^{i\hat{H}N\Delta t/\hbar} \right| \sigma_{i_N^-} \right\rangle. \tag{2.3}$$

The RDM for a general system initial condition $\tilde{\rho}^{(0)}_{i_0^\pm}$ is easily obtained from Eq. (2.3),

$$\tilde{\rho}^{(N)}_{i_N^\pm} \equiv {\rm Tr}_{\rm b} \left\langle \sigma_{i_N^+} \left| \hat{\rho}(N\Delta t) \right| \sigma_{i_N^-} \right\rangle = \sum_{i_0^\pm=1}^{n} U^{(N0)}_{i_N^\pm i_0^\pm} \tilde{\rho}^{(0)}_{i_0^\pm} \ . \tag{2.4}$$

Thus, the RP is the matrix of RDMs obtained with all possible single-term initial conditions.

Eq. (2.3) may be computed from a discretized path integral expression. Using a Trotter-type[40] factorization of the short-time propagator and evaluating the trace with respect to the bath degrees of freedom expresses the discretized path integral in the form

$$U^{(N0)}_{i_N^\pm i_0^\pm} = \sum_{i_{N-1}^\pm=1}^{n} \cdots \sum_{i_1^\pm=1}^{n} G_{i_N^\pm, i_{N-1}^\pm} \cdots G_{i_1^\pm, i_0^\pm} F_{i_N^\pm, i_{N-1}^\pm, \ldots, i_0^\pm} \tag{2.5}$$

where

$$G_{i_{k+1}^\pm, i_k^\pm} = \left\langle \sigma_{i_{k+1}^+} \left| e^{-i\hat{H}_0 \Delta t/\hbar} \right| \sigma_{i_k^+} \right\rangle \left\langle \sigma_{i_k^-} \left| e^{i\hat{H}_0 \Delta t/\hbar} \right| \sigma_{i_{k+1}^-} \right\rangle \tag{2.6}$$

are forward-backward system propagators of the (bare or renormalized) system Hamiltonian and F is the discretized Feynman-Vernon influence functional.[8] The influence functional is a complex exponential of the action that results from the force on the bath exerted by the system along a particular forward-backward path. If the bath is initially at a temperature $1/k_{\rm B}\beta$, the influence functional has the form[8]

$$F\left[s^{\pm}\right]=\exp\left[-\frac{1}{\hbar}\int_0^t dt'\int_0^{t'} dt''\left(s^{+}(t')-s^{-}(t')\right)\left(\alpha(t'-t'')s^{+}(t'')-\alpha^{*}(t'-t'')s^{-}(t'')\right)\right] \tag{2.7}$$

where s^{+},s^{-} are forward and backward paths of the system and $\alpha(t)$ is the force autocorrelation function of the bath. The discretized form of the influence functional depends on the factorization of the short-time evolution operator. For example, a crude asymmetric factorization leads to a rectangle-rule discretization of the two-dimensional integral, while a symmetric splitting produces a trapezoid rule discretization. The quasi-adiabatic propagator path integral[15] (QuAPI) employs a factorization based on the shifted system Hamiltonian along the adiabatic path, $\hat{H}_0=\hat{H}_{\rm sys}-\sum_j c_j{}^2\hat{s}^2/2m_j\omega_j^2$, i.e.

$$\hat{H}=\hat{H}_0+\sum_j\left(\frac{\hat{p}_j^2}{2m_j}+\frac{1}{2}m_j\omega_j^2\left(\hat{x}_j-\frac{c_j\hat{s}}{m_j\omega_j^2}\right)^2\right). \tag{2.8}$$

The QuAPI-discretized influence functional is given by the expression[38]

$$F_{i_N^{\pm},i_{N-1}^{\pm},\ldots,i_0^{\pm}}=F\left(s_N^{\pm},\ldots,s_0^{\pm}\right)=\exp\left[-\frac{1}{\hbar}\sum_{k'=0}^{N}\sum_{k''=0}^{k'}\left(s_{k'}^{+}-s_{k'}^{-}\right)\left(\eta_{k'k''}s_{k''}^{+}-\eta_{k'k''}^{*}s_{k''}^{-}\right)\right] \tag{2.9}$$

where the value of the system coordinate s_k^{+} at the time $k\Delta t$ on the forward path is $\sigma_{i_k^{+}}$, etc., and $\eta_{k'k''}$ are coefficients[17] related to integrals of the spectral density function,[5]

$$J(\omega)\equiv\frac{\pi}{2}\sum_j\frac{c_j^2}{m_j\omega_j}\delta\left(\omega-\omega_j\right)\ . \tag{2.10}$$

The influence functional coefficients may also be obtained directly from time correlation functions computed either quantum mechanically or via molecular dynamics simulations.[41] If the bath is initially in equilibrium with a particular site of the system, as in charge transfer reactions where the solvent is in equilibrium with the donor state, the influence functional contains additional terms,[42] but can be brought in the form of Eq. (2.9) through a system coordinate shift.[43] Eq. (2.9) is a product of two-time factors:

$$F_{i_N^{\pm},i_{N-1}^{\pm},\ldots,i_0^{\pm}}=\prod_{k'=1}^{N}\prod_{k''=1}^{k'}F_{i_{k'}^{\pm}i_{k''}^{\pm}}^{(k'k'')},\quad F_{i_{k'}^{\pm}i_{k''}^{\pm}}^{(k'k'')}=\exp\left[-\frac{1}{\hbar}\left(\sigma_{i_{k'}^{+}}-\sigma_{i_{k'}^{-}}\right)\left(\eta_{k'k''}\sigma_{i_{k''}^{+}}-\eta_{k'k''}^{*}\sigma_{i_{k''}^{-}}\right)\right]. \tag{2.11}$$

While the continuous-time influence functional expression, Eq. (2.7), is translationally invariant, the coefficients in the discretized form, Eq. (2.11), have been labeled with two indices, to indicate their different values near path endpoints. In particular, $\eta_{k'k''}=\eta_{k'-k''+1,1}\neq\eta_{k'-k'',0}$ if $1\le k',k''<N$, and $\eta_{N,k''}=\eta_{N-k'',0}$.

The time nonlocality encoded in the double sum in Eq. (2.9) entangles the path integral variables, and Eq. (2.5) requires the full evaluation of a sum with n^{2N} terms. However, the strength of these nonlocal interactions (i.e. the magnitude of the $\eta_{k'k''}$ coefficients) decays with increasing time separation $\Delta k=k'-k''$ and becomes negligible beyond some $\Delta k_{\max}$. Taking advantage of the finite length of these correlations,

the path sum may be evaluated iteratively[18] using a rank-$\Delta k_{\max}$ propagator tensor to connect the path segment $s^{\pm}_{k+\Delta k_{\max}-1},\ldots,s^{\pm}_{k}$ to $s^{\pm}_{k+\Delta k_{\max}},\ldots,s^{\pm}_{k+1}$. Thus, the iterative (i-QuAPI) decomposition reduces the exponential scaling with propagation length N to linear scaling. In its simplest form, the algorithm requires the storage of $n^{2\Delta k_{\max}}$ path amplitudes at each step, and each iteration involves $n^{2\Delta k_{\max}+2}$ operations, thus (in the absence of path elimination) the cost scales exponentially with the memory parameter $\Delta k_{\max}$. The algorithm has been extended to multiple coupled baths,[44] non-diagonal system-bath couplings,[31] Hamiltonians containing time-dependent fields[45] and equilibrium correlation functions.[46, 47]

The path integral time step Δt is to be made as large as allowed by the Trotter-type error in the factorization of the propagator. This error is sufficiently small if the discretized influence functional coefficients $\eta_{k'k''}$ are small, i.e. $|\eta_{k'k''}| \ll 1$. This restriction causes the influence functional factors $F^{(k'k'')}$ to be of order 1. The most important dissipative interactions are given by the diagonal factors $F^{(kk)}$, and $F^{(k'k'')}$ approach unity as $k'-k''$ increases.

III. Recursive removal of path integral entanglement

The RP at the first time point is given by the matrix $\mathbf{U}^{(10)}$ with elements

$$U^{(10)}_{i_1^{\pm} i_0^{\pm}} \equiv A^{(10)}_{i_1^{\pm} i_0^{\pm}} = F^{(11)}_{i_1^{\pm}} F^{(10)}_{i_1^{\pm} i_0^{\pm}} F^{(00)}_{i_0^{\pm}} G_{i_1^{\pm} i_0^{\pm}} \equiv M^{(10)}_{i_1^{\pm} i_0^{\pm}} . \tag{3.1}$$

Memory and temporal entanglement effects appear at later times. These effects are examined below.

(a) Single-step memory

If the bath-induced memory does not exceed a single path integral time step, i.e. $\Delta k_{\max} = 1$, then $F^{(k+2,k)}_{i_{k+2}^{\pm} i_k^{\pm}} = F^{(k+3,k)}_{i_{k+3}^{\pm} i_k^{\pm}} = \cdots = 0$. The RP at $2\Delta t$ is thus given by

$$U^{(20)}_{i_2^{\pm} i_0^{\pm}} = \sum_{i_1^{\pm}=1}^{n} F^{(22)}_{i_2^{\pm}} F^{(21)}_{i_2^{\pm} i_1^{\pm}} F^{(11)}_{i_1^{\pm}} F^{(10)}_{i_1^{\pm} i_0^{\pm}} F^{(00)}_{i_0^{\pm}} G_{i_2^{\pm} i_1^{\pm}} G_{i_1^{\pm} i_0^{\pm}} = \sum_{i_1^{\pm}=1}^{n} M^{(21)}_{i_2^{\pm} i_1^{\pm}} U^{(10)}_{i_1^{\pm} i_0^{\pm}} \quad , \tag{3.2}$$

where

$$M^{(k+1,k)}_{i_{k+1}^{\pm} i_k^{\pm}} \equiv A^{(k+1,k)}_{i_{k+1}^{\pm} i_k^{\pm}} \equiv F^{(k+1,k)}_{i_{k+1}^{\pm} i_k^{\pm}} F^{(kk)}_{i_k^{\pm}} G_{i_{k+1}^{\pm} i_k^{\pm}}, \quad k = 1,... \tag{3.3}$$

Similarly, the RP at the next time point is given by

$$U^{(30)}_{i_3^{\pm} i_0^{\pm}} = \sum_{i_2^{\pm}=1}^{n} \sum_{i_1^{\pm}=1}^{n} F^{(33)}_{i_3^{\pm}} F^{(32)}_{i_3^{\pm} i_2^{\pm}} G_{i_3^{\pm} i_2^{\pm}} F^{(22)}_{i_2^{\pm}} F^{(21)}_{i_2^{\pm} i_1^{\pm}} G_{i_2^{\pm} i_1^{\pm}} U^{(10)}_{i_1^{\pm} i_0^{\pm}} = \sum_{i_2^{\pm}=1}^{n} M^{(32)}_{i_3^{\pm} i_2^{\pm}} U^{(20)}_{i_2^{\pm} i_0^{\pm}} \quad . \tag{3.4}$$

The factorization of the double sum in Eq. (3.4) stems from the absence of influence functional couplings beyond adjacent time points. This factorization can be performed at later time points as well, thus the dynamics is Markovian in this case and the RP can be propagated by sequential multiplication of $n^2 \times n^2$ matrices,

$$\mathbf{U}^{(k+1,0)} = \mathbf{M}^{(k+1,k)} \cdot \mathbf{U}^{(k0)}, \quad k = 1,\ldots \tag{3.5}$$

However, even within the Markovian treatment, the propagator matrix $\mathbf{M}^{(k+1,k)}$ contains dissipative factors, and the corresponding RP eventually reaches its equilibrium value.

(b) Two-step memory

Next, consider the case of two-step memory, i.e. $\Delta k_{\max} = 2$. The RP dynamics is no longer Markovian in this case, although its structure is still sufficiently simple. Thus the case $\Delta k_{\max} = 2$ illustrates the entanglement and decomposition idea very clearly and is described in detail. The RP is given by

$$U^{(20)}_{i_2^{\pm} i_0^{\pm}} = \sum_{i_1^{\pm}=1}^{n} F^{(20)}_{i_2^{\pm} i_0^{\pm}} F^{(22)}_{i_2^{\pm}} F^{(21)}_{i_2^{\pm} i_1^{\pm}} F^{(11)}_{i_1^{\pm}} F^{(10)}_{i_1^{\pm} i_0^{\pm}} F^{(00)}_{i_0^{\pm}} G_{i_2^{\pm} i_1^{\pm}} G_{i_1^{\pm} i_0^{\pm}} = F^{(20)}_{i_2^{\pm} i_0^{\pm}} \sum_{i_1^{\pm}=1}^{n} M^{(21)}_{i_2^{\pm} i_1^{\pm}} U^{(10)}_{i_1^{\pm} i_0^{\pm}} \quad . \tag{3.6}$$

Eq. (3.6) involves a matrix product, as in the previous case, followed by multiplication of each element by the two-step influence functional factor. While this expression is in the desired form in terms of computational cost, it is useful to examine whether the RP can be brought in the form of a simple matrix product. Writing

$$F^{(20)}_{i_2^{\pm} i_0^{\pm}} = 1 + \left(F^{(20)}_{i_2^{\pm} i_0^{\pm}} - 1 \right), \tag{3.7}$$

Eq. (3.6) becomes

$$U^{(20)}_{i_2^{\pm} i_0^{\pm}} = \sum_{i_1^{\pm}=1}^{n} M^{(21)}_{i_2^{\pm} i_1^{\pm}} U^{(10)}_{i_1^{\pm} i_0^{\pm}} + M^{(20)}_{i_2^{\pm} i_0^{\pm}} , \tag{3.8}$$

where

$$M^{(20)}_{i_2^{\pm} i_0^{\pm}} \equiv \left(F^{(20)}_{i_2^{\pm} i_0^{\pm}} - 1 \right) \sum_{i_1^{\pm}=1}^{n} A^{(21)}_{i_2^{\pm} i_1^{\pm}} A^{(10)}_{i_1^{\pm} i_0^{\pm}} \quad . \tag{3.9}$$

Eq. (3.9) suggests that the RP at $2\Delta t$ differs from the matrix product $\mathbf{M}^{(21)} \cdot \mathbf{U}^{(10)}$ by the "remainder" matrix $\mathbf{M}^{(20)}$. The elements of this matrix are small, because the influence functional factors $F^{(20)}$ do not differ significantly from unity.

A graphical illustration of the RP matrix decomposition is shown in Figure 1. Each shaded shape corresponds to the two-time integrated region of the bath correlation function that gives rise to a particular influence functional factor. The three regions shaded in blue correspond to the influence functional factors included in $\mathbf{M}^{(10)}$, while the two regions shaded in yellow correspond to $\mathbf{M}^{(21)}$. The regions next to an endpoint have smaller areas because of the symmetric factorization of the short-time propagator.

The top panel illustrates the decomposition at $2\Delta t$. The matrix product $\mathbf{M}^{(21)} \cdot \mathbf{U}^{(10)}$ is obtained by linking the blue and orange regions. Subtraction of this product from $\mathbf{U}^{(20)}$ produces the remainder term where the reduced factor $F^{(20)} - 1$ is indicated as a patterned yellow region.

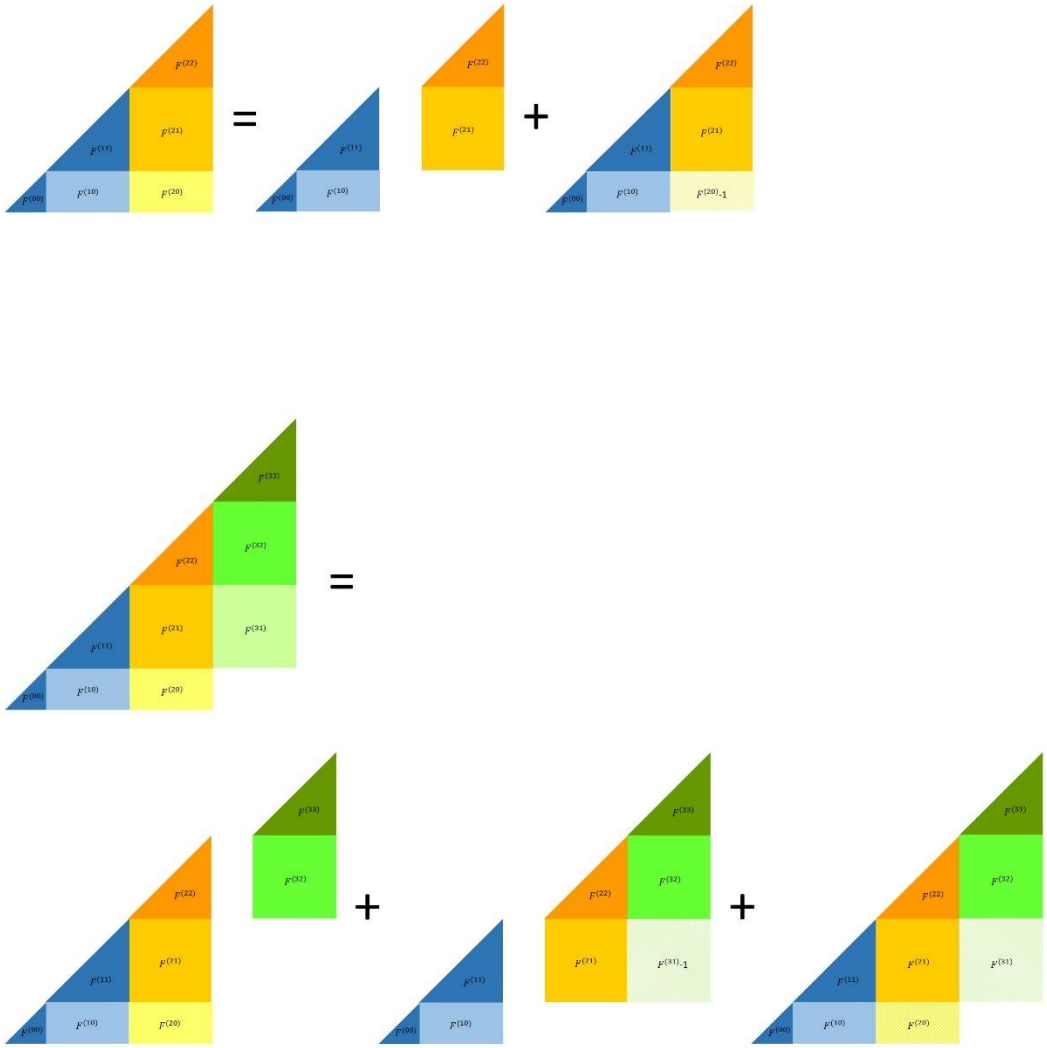

Fig. 1. Schematic illustration of the influence functional factors and matrix decomposition for the case of two-step memory. The path integral time step is equal to the length of a square. Each shaded region corresponds to the area included in an influence functional factor. Triangles correspond to $F^{(kk)}$ and solid-shaded squares correspond to $F^{(kk')}$. The blue group corresponds to the factors included in $\mathbf{M}^{(10)}$, the orange regions corresponds to those included in $\mathbf{M}^{(21)}$, the yellow rectangle corresponds to $\mathbf{M}^{(20)}$, the saturated green regions correspond to $\mathbf{M}^{(32)}$, and the pale green square shows $\mathbf{M}^{(31)}$. Hatched squares and rectangles correspond to $F^{(k+2,k)}-1$ factors. Top: decomposition of $\mathbf{U}^{(20)}$ according to Eq. (3.8). Bottom: decomposition of $\mathbf{U}^{(30)}$ according to Eq. (3.14).

At the next time step $3\Delta t$, the RP with $\Delta k_{\max} = 2$ is given by the expression

$$U^{(30)}_{i_3^{\pm} i_0^{\pm}} = \sum_{i_2^{\pm}=1}^{n} \sum_{i_1^{\pm}=1}^{n} F^{(31)}_{i_3^{\pm} i_1^{\pm}} F^{(20)}_{i_2^{\pm} i_0^{\pm}} A^{(32)}_{i_3^{\pm} i_2^{\pm}} A^{(21)}_{i_2^{\pm} i_1^{\pm}} A^{(10)}_{i_1^{\pm} i_0^{\pm}} \ . \tag{3.10}$$

Eq. (3.10) contains a double sum that cannot be factored into single sums, which is a manifestation of the two-step influence functional entanglement.

Motivated by the matrix product decomposition in the case of $\Delta k_{\max} = 1$ and the typically smaller magnitude of two-step influence functional memory, one realizes that the product form of Eq. (3.4) must constitute the dominant contribution to Eq. (3.10). Following the previous procedure, this matrix product appears by decomposing the two-step influence functional factor as $1 + (F^{(31)}_{i_3^{\pm} i_1^{\pm}} - 1)$. This procedure brings the RP to the form

$$U^{(30)}_{i_3^{\pm} i_0^{\pm}} = \sum_{i_2^{\pm}=1}^{n} M^{(32)}_{i_3^{\pm} i_2^{\pm}} U^{(20)}_{i_2^{\pm} i_0^{\pm}} + \sum_{i_2^{\pm}=1}^{n} \sum_{i_1^{\pm}=1}^{n} \left(F^{(31)}_{i_3^{\pm} i_1^{\pm}} - 1 \right) F^{(20)}_{i_2^{\pm} i_0^{\pm}} A^{(32)}_{i_3^{\pm} i_2^{\pm}} A^{(21)}_{i_2^{\pm} i_1^{\pm}} A^{(10)}_{i_1^{\pm} i_0^{\pm}} \ . \tag{3.11}$$

Next, the factor $F^{(20)}_{i_2^{\pm} i_0^{\pm}}$ in the second term of Eq. (3.11) prevents its factorization. In the absence of this factor, this term would become a matrix product,

$$\sum_{i_2^{\pm}=1}^{n} \sum_{i_1^{\pm}=1}^{n} \left(F^{(31)}_{i_3^{\pm} i_1^{\pm}} - 1 \right) A^{(32)}_{i_3^{\pm} i_2^{\pm}} A^{(21)}_{i_2^{\pm} i_1^{\pm}} A^{(10)}_{i_1^{\pm} i_0^{\pm}} = \sum_{i_1^{\pm}=1}^{n} M^{(31)}_{i_3^{\pm} i_1^{\pm}} U^{(10)}_{i_1^{\pm} i_0^{\pm}} \ , \tag{3.12}$$

where $\mathbf{M}^{(31)}$ is an $n^2 \times n^2$ two-step propagator matrix analogous to $\mathbf{M}^{(20)}$. The elements of this matrix are given by

$$M^{(31)}_{i_3^{\pm} i_1^{\pm}} \equiv \left(F^{(31)}_{i_3^{\pm} i_1^{\pm}} - 1 \right) \sum_{i_2^{\pm}=1}^{n} A^{(32)}_{i_3^{\pm} i_2^{\pm}} A^{(21)}_{i_2^{\pm} i_1^{\pm}} \ . \tag{3.13}$$

To achieve the factorization of Eq. (3.12), the other two-step influence functional factor is written as $1 + (F^{(20)}_{i_2^{\pm} i_0^{\pm}} - 1)$. This leads to the decomposition

$$U^{(30)}_{i_3^{\pm} i_0^{\pm}} = \sum_{i_2^{\pm}=1}^{n} M^{(32)}_{i_3^{\pm} i_2^{\pm}} U^{(20)}_{i_2^{\pm} i_0^{\pm}} + \sum_{i_1^{\pm}=1}^{n} M^{(31)}_{i_3^{\pm} i_1^{\pm}} U^{(10)}_{i_1^{\pm} i_0^{\pm}} + M^{(30)}_{i_3^{\pm} i_0^{\pm}} \ , \tag{3.14}$$

where

$$M^{(30)}_{i_3^{\pm} i_0^{\pm}} = \sum_{i_2^{\pm}=1}^{n} \sum_{i_1^{\pm}=1}^{n} \left(F^{(31)}_{i_3^{\pm} i_1^{\pm}} - 1 \right) \left(F^{(20)}_{i_2^{\pm} i_0^{\pm}} - 1 \right) A^{(32)}_{i_3^{\pm} i_2^{\pm}} A^{(21)}_{i_2^{\pm} i_1^{\pm}} A^{(10)}_{i_1^{\pm} i_0^{\pm}} \ . \tag{3.15}$$

The matrix decomposition at $3\Delta t$ for the case $\Delta k_{\max} = 2$ is illustrated in the bottom panel of Fig. 1.

The matrix $\mathbf{M}^{(30)}$ is the remainder of the RP factorization at $3\Delta t$. Its structure is similar to that of the full path sum for the RP, Eq. (3.10), and evaluation of this term requires a double sum. However, the magnitude of $\mathbf{M}^{(30)}$ is significantly diminished, since

$$\left(F^{(31)}_{i_3^{\pm}i_1^{\pm}}-1\right)\left(F^{(20)}_{i_2^{\pm}i_0^{\pm}}-1\right)=\left(e^{-\frac{1}{\hbar}\left(\sigma_{i_3^{+}}-\sigma_{i_3^{-}}\right)\left(\eta_{31}\sigma_{i_1^{+}}-\eta^{*}_{31}\sigma_{i_1^{-}}\right)}-1\right)\left(e^{-\frac{1}{\hbar}\left(\sigma_{i_2^{+}}-\sigma_{i_2^{-}}\right)\left(\eta_{20}\sigma_{i_0^{+}}-\eta^{*}_{20}\sigma_{i_0^{-}}\right)}-1\right) \tag{3.16}$$

and the two-step influence functional coefficients have small values.

Continuing to the fourth time step, the full path sum with $\Delta k_{\max}=2$ influence functional terms has the form

$$U^{(40)}_{i_4^{\pm}i_0^{\pm}}=\sum_{i_3^{\pm}=1}^{n}\sum_{i_2^{\pm}=1}^{n}\sum_{i_1^{\pm}=1}^{n}F^{(42)}_{i_4^{\pm}i_2^{\pm}}F^{(31)}_{i_3^{\pm}i_1^{\pm}}F^{(20)}_{i_2^{\pm}i_0^{\pm}}A^{(43)}_{i_3^{\pm}i_2^{\pm}}A^{(32)}_{i_3^{\pm}i_2^{\pm}}A^{(21)}_{i_2^{\pm}i_1^{\pm}}A^{(10)}_{i_1^{\pm}i_0^{\pm}} \tag{3.17}$$

Proceeding as before, it is straightforward to show that Eq. (3.17) can be factored in the form

$$U^{(40)}_{i_4^{\pm}i_0^{\pm}}=\sum_{i_3^{\pm}=1}^{n}M^{(43)}_{i_4^{\pm}i_3^{\pm}}U^{(30)}_{i_3^{\pm}i_0^{\pm}}+\sum_{i_2^{\pm}=1}^{n}M^{(42)}_{i_4^{\pm}i_2^{\pm}}U^{(20)}_{i_2^{\pm}i_0^{\pm}}+\sum_{i_1^{\pm}=1}^{n}M^{(41)}_{i_4^{\pm}i_1^{\pm}}U^{(10)}_{i_1^{\pm}i_0^{\pm}}+M^{(40)}_{i_4^{\pm}i_0^{\pm}} \tag{3.18}$$

where $\mathbf{M}^{(42)}=\mathbf{M}^{(31)}$,

$$M^{(41)}_{i_4^{\pm}i_1^{\pm}}=\sum_{i_3^{\pm}=1}^{n}\sum_{i_2^{\pm}=1}^{n}\left(F^{(42)}_{i_4^{\pm}i_2^{\pm}}-1\right)\left(F^{(31)}_{i_3^{\pm}i_1^{\pm}}-1\right)A^{(43)}_{i_4^{\pm}i_3^{\pm}}A^{(32)}_{i_3^{\pm}i_2^{\pm}}A^{(21)}_{i_2^{\pm}i_1^{\pm}} \tag{3.19}$$

and the remainder matrix has elements

$$M^{(40)}_{i_4^{\pm}i_0^{\pm}}=\sum_{i_3^{\pm}=1}^{n}\sum_{i_2^{\pm}=1}^{n}\sum_{i_1^{\pm}=1}^{n}\left(F^{(42)}_{i_4^{\pm}i_2^{\pm}}-1\right)\left(F^{(31)}_{i_3^{\pm}i_1^{\pm}}-1\right)\left(F^{(20)}_{i_2^{\pm}i_0^{\pm}}-1\right)A^{(43)}_{i_4^{\pm}i_3^{\pm}}A^{(32)}_{i_3^{\pm}i_2^{\pm}}A^{(21)}_{i_2^{\pm}i_1^{\pm}}A^{(10)}_{i_1^{\pm}i_0^{\pm}}\,. \tag{3.20}$$

Eq. (3.18) is an exact decomposition of the RP at $4\Delta t$. It is written in terms of single- and multi-step propagator matrices, as well as the RP at the earlier time points. The single-step propagators are given by Eq. (3.3). The two-step propagator matrices $\mathbf{M}^{(42)}=\mathbf{M}^{(31)}$ have the same form as the $2\Delta t$ remainder matrix $\mathbf{M}^{(20)}$, but the values of their elements differ, because $\mathbf{A}^{(21)}\neq\mathbf{A}^{(10)}$. Similarly, the three-step propagator matrix $\mathbf{M}^{(41)}$ has a form that is similar to the $3\Delta t$ remainder matrix $\mathbf{M}^{(30)}$. The entanglement of the original path integral expression is buried in these matrices. Because of the exact nature of Eq. (3.20), the path integral variable at the time point $4\Delta t$ is (indirectly) coupled to (i.e. entangled with) the variable at $t=0$ in the remainder matrix $\mathbf{M}^{(40)}$, and one needs to evaluate the full triple sum in order to compute its elements, even though the memory length has been assumed equal to two time steps.

One can proceed along the same lines to obtain an exact decomposition of the RP at subsequent time points. In each case, an exact evaluation of the remainder term would require the same number of operations as the original path integral expression. However, the decreasing magnitude of the remainder

terms, Equations (3.9), (3.15) and (3.20) suggests that these terms will quickly become negligible, allowing truncation of the hierarchy. This behavior is discussed extensively in the next section.

(c) Three-step memory

Next, consider the inclusion of $\Delta k_{\max} = 3$ terms in the path integral, which enter at $3\Delta t$ and beyond. The RP at $3\Delta t$ is now given by

$$U^{(30)}_{i_3^{\pm} i_0^{\pm}} = F^{(30)}_{i_3^{\pm} i_0^{\pm}} \sum_{i_2^{\pm}=1}^{n} \sum_{i_1^{\pm}=1}^{n} F^{(31)}_{i_3^{\pm} i_1^{\pm}} F^{(20)}_{i_2^{\pm} i_0^{\pm}} A^{(32)}_{i_3^{\pm} i_2^{\pm}} A^{(21)}_{i_2^{\pm} i_1^{\pm}} A^{(10)}_{i_1^{\pm} i_0^{\pm}} \,. \tag{3.21}$$

Its decomposition is again given by Eq. (3.14). Since the three-step influence functional factor cannot enter in the one- and two-step propagators, it should only affect the remainder term. Adding and subtracting unity as done earlier, one finds

$$M^{(30)}_{i_3^{\pm} i_0^{\pm}} = \sum_{i_2^{\pm}=1}^{n} \sum_{i_1^{\pm}=1}^{n} \left[\left(F^{(31)}_{i_3^{\pm} i_1^{\pm}} - 1 \right) \left(F^{(20)}_{i_2^{\pm} i_0^{\pm}} - 1 \right) + \left(F^{(30)}_{i_3^{\pm} i_0^{\pm}} - 1 \right) F^{(31)}_{i_3^{\pm} i_1^{\pm}} F^{(20)}_{i_2^{\pm} i_0^{\pm}} \right] A^{(32)}_{i_3^{\pm} i_2^{\pm}} A^{(21)}_{i_2^{\pm} i_1^{\pm}} A^{(10)}_{i_1^{\pm} i_0^{\pm}} \,. \tag{3.22}$$

One now observes two contributions to the remainder matrix $\mathbf{M}^{(30)}$: the contribution from the entangled two-step influence functional factors, Eq. (3.15), and a new term that includes the three-step memory factor $F^{(30)}$. Since this second term contains a single factor where unity is subtracted, while the first term contains two such factors, it is evident that the three-step memory term is the dominant contribution to the remainder matrix $\mathbf{M}^{(30)}$.

The decomposition of $\mathbf{U}^{(40)}$ has the form of Eq. (3.18), with the three-step propagator given by an expression analogous to Eq. (3.22), i.e.,

$$M^{(41)}_{i_4^{\pm} i_1^{\pm}} = \sum_{i_3^{\pm}=1}^{n} \sum_{i_2^{\pm}=1}^{n} \left[\left(F^{(42)}_{i_4^{\pm} i_2^{\pm}} - 1 \right) \left(F^{(31)}_{i_3^{\pm} i_1^{\pm}} - 1 \right) + \left(F^{(41)}_{i_4^{\pm} i_1^{\pm}} - 1 \right) F^{(42)}_{i_4^{\pm} i_2^{\pm}} F^{(31)}_{i_3^{\pm} i_1^{\pm}} \right] A^{(43)}_{i_4^{\pm} i_3^{\pm}} A^{(32)}_{i_3^{\pm} i_2^{\pm}} A^{(21)}_{i_2^{\pm} i_1^{\pm}} \,. \tag{3.23}$$

Proceeding as at the previous time point, one can obtain the new remainder matrix $\mathbf{M}^{(40)}$, modified through the inclusion of three-step influence functional factors:

$$\begin{aligned} M^{(40)}_{i_4^{\pm} i_0^{\pm}} = \sum_{i_3^{\pm}=1}^{n} \sum_{i_2^{\pm}=1}^{n} \sum_{i_1^{\pm}=1}^{n} A^{(43)}_{i_4^{\pm} i_3^{\pm}} A^{(32)}_{i_3^{\pm} i_2^{\pm}} A^{(21)}_{i_2^{\pm} i_1^{\pm}} A^{(10)}_{i_1^{\pm} i_0^{\pm}} \Big[& \left(F^{(42)}_{i_4^{\pm} i_2^{\pm}} - 1 \right) \left(F^{(31)}_{i_3^{\pm} i_1^{\pm}} - 1 \right) \left(F^{(20)}_{i_2^{\pm} i_0^{\pm}} - 1 \right) \\ & + F^{(42)}_{i_4^{\pm} i_2^{\pm}} F^{(31)}_{i_3^{\pm} i_1^{\pm}} \left(F^{(41)}_{i_4^{\pm} i_1^{\pm}} - 1 \right) \left(F^{(20)}_{i_2^{\pm} i_0^{\pm}} - 1 \right) + F^{(31)}_{i_3^{\pm} i_1^{\pm}} F^{(20)}_{i_2^{\pm} i_0^{\pm}} \left(F^{(30)}_{i_3^{\pm} i_0^{\pm}} - 1 \right) \left(F^{(42)}_{i_4^{\pm} i_2^{\pm}} - 1 \right) \\ & + F^{(42)}_{i_4^{\pm} i_2^{\pm}} F^{(31)}_{i_3^{\pm} i_1^{\pm}} F^{(20)}_{i_2^{\pm} i_0^{\pm}} \left(F^{(41)}_{i_4^{\pm} i_1^{\pm}} - 1 \right) \left(F^{(30)}_{i_3^{\pm} i_0^{\pm}} - 1 \right) \Big] \end{aligned} \tag{3.24}$$

Again, the remainder $\mathbf{M}^{(40)}$ is expected to be smaller than $\mathbf{M}^{(30)}$, since each term in Eq. (3.24) contains two or more small $(F^{(k'k'')} - 1)$ factors. Further, the only term in Eq. (3.24) that does not include three-step influence functional terms (i.e. the term given by Eq. (3.20)) contains three small factors, while the other terms contain only two such factors. Thus the dominant contribution to $\mathbf{M}^{(40)}$ arises from the three-step memory and not from the leftover two-step entanglement term.

By proceeding along these lines, one can decompose the RP for any number of time steps and any memory length.

IV. Decay of entanglement and hierarchy truncation

The previous section showed that the RP at the time $r\Delta t$ can be decomposed in the following form,

$$\mathbf{U}^{(r0)} = \sum_{m=1}^{r-1} \mathbf{M}^{(rm)} \cdot \mathbf{U}^{(m0)} + \mathbf{M}^{(r0)}, \quad r = 1,\ldots \tag{4.1}$$

where $\mathbf{M}^{(rm)}$ are $n^2 \times n^2$ matrices obtainable in terms of sums that involve the system propagator as well as influence functional factors.

Each term in Eq. (4.1) couples the two endpoints through a single path integral variable, i.e. the entanglement present in the original path integral expression is now buried in the $\mathbf{M}^{(rm)}$ matrices. Since $\mathbf{M}^{(rm)}$ involves an $(r-m-1)$-dimensional sum, there is partial entanglement encoded in these matrices. The remainder matrix contains the full variable entanglement of the original RDM expression, and the effort required for its exact evaluation is identical to the effort required for computing the original discretized path integral.

However, for a fixed memory length, the magnitude of the remainder term decays rapidly with *r*. This trend is born out of the analytical forms obtained for small *r* values in the previous section, where it was seen that for fixed $\Delta k_{\max}$ the elements of $\mathbf{M}^{(r0)}$ are multiplied by more small factors as *r* increases. This decreasing nature of $\mathbf{M}^{(r0)}$, which is further analyzed below and in subsequent sections, invites truncation of the hierarchy in Eq. (4.1). One can define a *temporal entanglement length* $r_{\max}$, such that the elements of the remainder matrix $\mathbf{M}^{(r0)}$ are negligible for $r \geq r_{\max}$. This value can be thought of as the length of entangled interactions that must be accounted for to recover (within the desired accuracy) the full path integral result. In analogy to the memory parameter $\Delta k_{\max}$, the entanglement length $r_{\max}$ can be treated as a convergence parameter. Nevertheless, it is of interest to obtain an estimate of the entanglement length that must be treated for accurate results.

A useful suggestion is given by the forms given and discussed in the previous section, where it was seen that the dominant contribution to $\mathbf{M}^{(r0)}$ arises from $\Delta k_{\max} = r$ influence functional factors, and that the entangled contribution of $\Delta k_{\max} < r$ terms tends to be small and decreases rapidly with increasing *r*. Thus, one suspects that the choice $r_{\max} = \Delta k_{\max}$ may generally be sufficiently accurate.

Additional useful insights can be obtained analytically using the spin-boson ($n = 2$) model.[6] At zero temperature the bath autocorrelation function is given by

$$\alpha(t) = \pi^{-1} \int_0^\infty J(\omega) e^{-i\omega t} d\omega \tag{4.2}$$

and for an Ohmic spectral density,[5]

$$J(\omega) = \frac{\pi}{2} \left(\frac{2}{\Delta\sigma} \right)^2 \hbar\omega\xi \, e^{-\omega/\omega_c} \tag{4.3}$$

(where $\Delta\sigma \equiv \sigma_n - \sigma_1 = 2$), the influence functional coefficients can be evaluated analytically. Using the expressions for the influence functional coefficients in terms of double time integrals of the bath autocorrelation function,[41] one finds

$$\eta_{k'k''} = \frac{1}{2}\left(\frac{2}{\Delta\sigma}\right)^2 \hbar\xi \ln \frac{1 + 2i\,\Delta k\,\omega_c\Delta t - \left(\Delta k^2 - 1\right)\left(\omega_c\Delta t\right)^2}{\left(1 + i\,\Delta k\,\omega_c\Delta t\right)^2} \tag{4.4}$$

where $\Delta k \equiv k' - k'' > 1$, as long as k', k'' are not path endpoints.

If the time step is small compared to the bath relaxation time given by ω_c^{-1}, one may expand the influence functional factors in the small parameter $\omega_c\Delta t$. Suppose the memory is truncated at $\Delta k_{\max} = 2$. For $\xi = \frac{1}{2}$ and $s_{k'} - s_{k''} = 2$, the leading term (i.e. the real part of the exponent) in the two-step ($r = 2$) propagator matrix $M^{(31)}$ that appears in Eq. (3.13) is $e^{-4\eta_{31}} - 1 \simeq -(\omega_c\Delta t)^2$, while the corresponding term in the three-step ($r = 3$) propagator $M^{(41)}$ is $(e^{-4\eta_{42}} - 1)(e^{-4\eta_{31}} - 1) \simeq (\omega_c\Delta t)^4$. Thus, the contribution of the $r = 3$ term is small for $\Delta k_{\max} = 2$. Retaining the $\Delta k_{\max} = 3$ factors adds to the $M^{(41)}$ ($r = 3$) element a term of order $e^{-4\eta_{41}} - 1 \simeq -(\omega_c\Delta t)^2$, which is comparable to the $\Delta k_{\max} = 2$, $r = 2$ matrix element. However, the $r = 4$ terms contained in $M^{(51)}$ are again reduced by a factors $e^{-4\eta_{31}} - 1$ or $e^{-4\eta_{41}} - 1 \simeq -(\omega_c\Delta t)^2$, so they are again of order $(\omega_c\Delta t)^4$. One sees that with $\Delta k_{\max} = 3$, inclusion of the $r = 4$ term makes a negligible contribution.

Further evidence is offered by numerical calculations on spin-boson models. The SMatPI matrices for a symmetric TLS with 'typical' parameters (a moderate memory length) were presented in Ref. [39]. The present paper employs an asymmetric TLS described by the Hamiltonian

$$\hat{H}_0 = -\hbar\Omega\left(|\sigma_1\rangle\langle\sigma_2| + |\sigma_2\rangle\langle\sigma_1|\right) + \varepsilon\left(|\sigma_1\rangle\langle\sigma_1| - |\sigma_2\rangle\langle\sigma_2|\right) \tag{4.5}$$

with coordinates $\sigma_1 = 1, \sigma_2 = -1$ and asymmetry parameter $\varepsilon = \hbar\Omega$. The TLS is coupled to a dissipative harmonic bath as in Eq. (2.8) with an Ohmic spectral density characterized by $\omega_c = 2\Omega$ and $\xi = 2$ at a low temperature corresponding to $\hbar\Omega\beta = 5$. The peak of the bath spectral density is resonant with the left-right coupling matrix element and smaller than the TLS level splitting (which is equal to $2\sqrt{2}\,\hbar\Omega$). The strongly coupled sluggish bath gives rise to interesting modulations of the RDM elements, as well as interesting memory effects. As shown in the results presented in the next section, converged results for the RDM are obtained with $\Omega\Delta t = 0.125$ and $\Delta k_{\max} = 15$. For a TLS, the SMatPI decomposition involves 4×4 matrices.

Figure 2 shows the magnitude of $M_{12,12}^{(r+1.1)}$ for $r = \Delta k_{\max}$, $r = \Delta k_{\max} + 1$ and $r = \Delta k_{\max} + 2$ for several values of the memory length parameter $\Delta k_{\max}$. It is seen that for each value of $\Delta k_{\max}$, the element of this matrix drops rapidly when r is increased from $\Delta k_{\max}$ to $\Delta k_{\max} + 1$, and is further decreased when $r = \Delta k_{\max} + 2$. It is also seen that the value of $M_{12,12}^{(r0)}$ jumps to a larger value upon increasing $\Delta k_{\max}$ from $r - 1$ to r, confirming again the dominant nature of influence functional memory compared to the smaller memory entangled remainder contribution. (A small irregularity is observed at $r = \Delta k_{\max} = 4$, where the matrix element is unexpectedly small; this arises because the bath correlation function and the influence functional coefficient change from positive to negative values around that time, causing the false impression of almost vanishing memory contribution.)

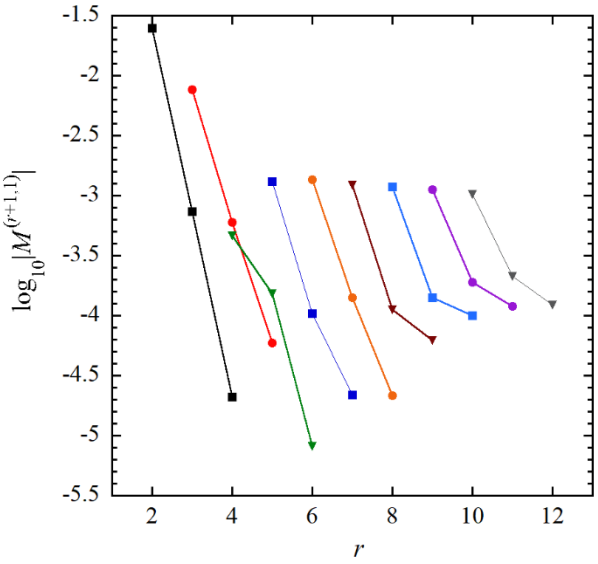

Fig. 2. Absolute value of $M_{12,12}^{(r+1,1)}$ for $r=\Delta k_{\max}, \Delta k_{\max}+1$ and $\Delta k_{\max}+2$ as a function of r for the asymmetric TLS described in section IV. The lines connect values corresponding to the same $\Delta k_{\max}$. From left to right, the curves correspond to $\Delta k_{\max}=2,3,\ldots,8$.

The properties of a matrix are best understood by examining its eigenvalues. The properties of the SMatPI matrices are discussed in the next section, where it is shown that for a TLS, the 4×4 propagator matrices $\mathbf{M}^{(r0)}$ with $r\geq 2$ have two nonzero eigenvalues which are either real or complex conjugates of each other. Figure 3 shows the largest (in absolute value) eigenvalue of $\mathbf{M}^{(\Delta k_{\max}+1,1)}$ ($r=\Delta k_{\max}$) and of $\mathbf{M}^{(\Delta k_{\max}+2,1)}$ ($r=\Delta k_{\max}+1$). One observes again that the matrix with $r=\Delta k_{\max}$ has considerably larger eigenvalues compared to that with $r=\Delta k_{\max}+1$. The non-monotonic behavior observed at $r=\Delta k_{\max}=4$ and 10 is again a consequence of the oscillatory nature of the bath correlation function, which causes the influence functional coefficients to change sign around these values of memory length. Thus, truncating the SMatPI hierarchy at $r_{\max}=\Delta k_{\max}$ should generally lead to error that is smaller than the error due to memory truncation. (One could, of course, use a somewhat larger value of $r_{\max}$ in order to verify convergence.) Eventually, as the necessary memory length is reached, both contributions from entanglement and memory truncation become negligible, and the remainder term can be omitted.

Dropping the negligible multistep propagator matrices beyond the entanglement length $r_{\max}$ allows truncation of Eq. (4.1),

$$\mathbf{U}^{(N0)}=\sum_{r=1}^{r_{\max}}\mathbf{M}^{(N,N-r)}\cdot\mathbf{U}^{(N-r,0)},\quad N=r_{\max}+1,\ldots \tag{4.6}$$

The SMatPI matrices are evaluated recursively from Eq. (4.1), noting that $\mathbf{M}^{(N,N-r)}=\mathbf{M}^{(r+1,1)}$ would be obtained from the expression for $\mathbf{M}^{(r0)}$ if the influence functional coefficients η_{k0} are replaced by $\eta_{k+1,1}$. Adopting this substitution and starting with $\mathbf{M}^{(21)}$ and the RP values $\mathbf{U}^{(10)}$ and $\mathbf{U}^{(20)}$, one obtains $\mathbf{M}^{(20)}$ by subtraction according to Eq. (3.8), which is equal to the required propagation matrix $\mathbf{M}^{(31)}$. Next, using

this matrix and $\mathbf{M}^{(32)} = \mathbf{M}^{(21)}$, along with the RP matrix $\mathbf{U}^{(30)}$, one obtains from Eq. (3.14) the remainder matrix $\mathbf{M}^{(30)}$, which (again by virtue of the proper influence functional coefficients) is the SMatPI matrix $\mathbf{M}^{(41)}$. This procedure is extremely straightforward and may be performed numerically to generate all SMatPI matrices required for propagation beyond the entanglement length according to Eq. (4.6). The most time consuming part in this process is the calculation of $\mathbf{M}^{(N,N-r_{\max})} = \mathbf{M}^{(r_{\max}+1,1)}$, which is obtained by evaluating $\mathbf{M}^{(r_{\max},0)}$ with midpoint influence functional coefficients, and thus involves a single $(r_{\max}-1)$-dimensional sum for each of the n^4 elements. Once these matrices have been computed, propagation according to Eq. (4.6) scales linearly with time and is extremely fast, as it involves just ordinary multiplications and additions of $n^2 \times n^2$ matrices.

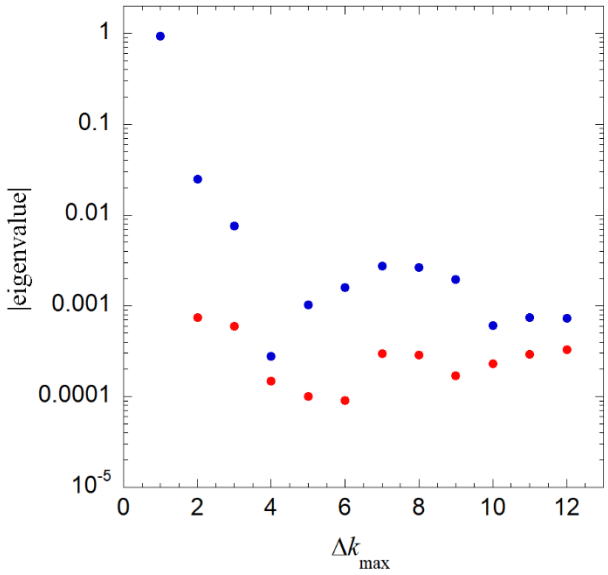

Fig. 3. Absolute value of the largest eigenvalue of $\mathbf{M}^{(r0)}$ for $r_{\max} = \Delta k_{\max}$ and $r_{\max} = \Delta k_{\max} + 1$ as a function of $\Delta k_{\max}$ for the asymmetric TLS described in the section IV.

V. Structure and properties of SMatPI matrices

Each column of Eq. (4.6) gives the RDM for a particular initial condition, thus the $\mathbf{M}^{(Nm)}$ matrices couple the RDM at the time $N\Delta t$ to the RDM at the earlier times. This structure is reminiscent of the Nakajima-Zwanzig generalized master equation[48] (GQME), where the time derivative of the RDM depends on the RDM history through a simple time integral. In fact, Eq. (4.6) bears a close resemblance to the transfer tensor scheme[49] (TTM), which in the $\Delta t \to 0$ limit is equivalent to the GQME.

However, the hierarchy obtained through the SMatPI decomposition differs in important ways from the TTM/GQME hierarchy. The latter employs translationally invariant matrices $\mathbf{T}^{(N,N-r)} = \mathbf{T}^{(r0)}$. Such a form appears compatible with the path integral only through a crude, unsymmetrized Trotter splitting of the propagators, which is accurate in the limit $\Delta t \to 0$. The influence functional structure shown in Fig. 1 and the SMatPI derivation given in section III show clearly that the small matrix decomposition of the RP must employ different matrices at endpoints, i.e. $\mathbf{M}^{(r+1,1)} \neq \mathbf{M}^{(r0)}$. The TTM/GQME matrices, which lack this

flexibility, have a different structure and larger elements than the SMatPI matrices, i.e. they include a spurious memory and decay slower.

The eigenvalue analysis of the propagator matrices can offer useful insights. The information contained in the set of $r \simeq \Delta k_{\max}$ SMatPI matrices is equivalent to that contained in the i-QuAPI propagator tensor.[17, 18] The latter has $n^{2(\Delta k_{\max}+1)}$ eigenvectors and eigenvalues, although the majority of i-QuAPI tensor eigenvalues are zero. The eigenvalue analysis is much more conveniently and economically performed through the small SMatPI matrices.

The single step SMatPI matrices $\mathbf{M}^{(10)}$ and $\mathbf{M}^{(k+1,k)}$ have only nonzero eigenvalues, of which one equals unity. From Eq. (2.11), one sees that $F^{(k'k'')}_{i^{\pm}_{k'}i^{\pm}_{k''}} = 1$ if $i^{+}_{k'} = i^{-}_{k'}$. Because of the $(F^{(N,N-r)}_{i^{\pm}_{N}i^{\pm}_{N-r}} - 1)$ factors, the matrix elements of $\mathbf{M}^{(N,N-r)}$ for $r > 1$ have n rows equal to zero. Thus the only direct contribution to $\mathbf{U}^{(N0)}_{i^{\pm}_{N},0}$ (i.e. to the diagonal elements of the RDM) comes from the single-step matrix $\mathbf{M}^{(N,N-1)}$. The presence of n rows with vanishing elements in the SMatPI matrices $\mathbf{M}^{(N,N-r)}$ for $r > 1$ implies that these matrices have n zero eigenvalues. The remaining $n^2 - n$ eigenvalues are either real-valued of form complex conjugate pairs.

VI. Representative applications

This section illustrates the SMatPI decomposition by simulating the dynamics of several model dissipative systems.

The first model system is given by the Hamiltonian of Eq. (4.5). Figure 4 shows the time evolution of the diagonal and off-diagonal elements of the RDM with the initial condition initial condition $\tilde{\rho} = |\sigma_1\rangle\langle\sigma_1|$ (and the bath initially at thermal equilibrium). Shown are converged full-memory results obtained with $\Delta k_{\max} = 15$, as well as results obtained with the Markovian-like, single-step memory treatment $\Delta k_{\max} = 1$.

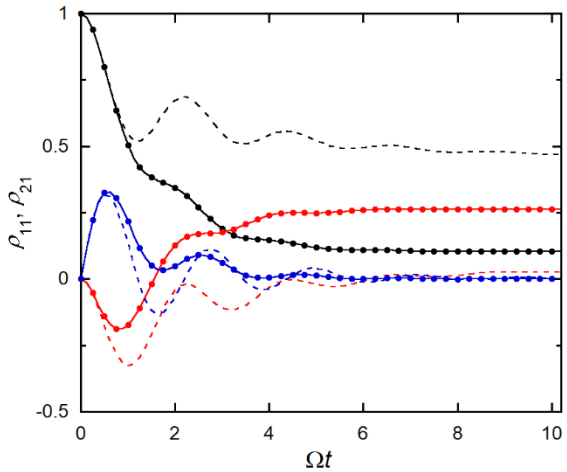

Fig. 4. Reduced density matrix elements for the asymmetric TLS discussed in section VI (with parameters given in section IV). The solid lines and filled markers show converged results obtained with $\Delta k_{\max} = 15$, while the dashed lines show results with $\Delta k_{\max} = 1$. Black: diagonal RDM element corresponding to population of state 1. Red and blue: real and imaginary parts of off-diagonal element $\tilde{\rho}_{21}$.

As seen in the figure, the Markovian results are very poor. The population exhibits quenched oscillations and reaches and incorrect long-time value. Strong oscillatory patterns are observed in the off-diagonal element as well, whose real part also reaches an incorrect long-time value. This behavior can be traced to the propagator matrix $\mathbf{M}^{(21)}$, which is responsible for the time evolution after the first time step. This matrix has a unit eigenvalue, a pair of complex conjugate eigenvalues and a single real eigenvalue smaller than unity. The complex eigenvalues are responsible for the oscillatory pattern, while the real eigenvalue is associated with the observed decay.

Upon including more memory through $\mathbf{M}^{(N,N-\Delta k)}$ matrices with $\Delta k \geq 2$, the RDM elements become less oscillatory. The shoulder regions observed in the converged results are remnants of the $\Delta k_{\max} = 1$ oscillatory behavior. The multi-step propagator matrices modify the dynamics in two ways, by modulating the frequency components of the $\Delta k_{\max} = 1$ result and through gradual damping. These effects are encoded in the eigenvalues and eigenvectors of these matrices. With the given parameters, approximately the first half of these matrices has two small complex eigenvalues, which alter slightly the oscillatory pattern, while the rest have small real eigenvalues, which modify the decay characteristics.

Figure 5 investigates the effect of the entanglement length on the RDM dynamics. Shown are the values of the diagonal and off-diagonal RDM elements obtained with $\Delta k_{\max} = 5$ and 10, with entanglement lengths given by $r_{\max} = \Delta k_{\max}$ and $r_{\max} = \Delta k_{\max} + 1$. In the case of $\Delta k_{\max} = 5$, for which the memory is truncated very early, the $r_{\max} = \Delta k_{\max}$ results exhibit a small error at long times which is about 0.006. The $\Delta k_{\max} = 10$, which include most of the memory, are very well converged with $r_{\max} = \Delta k_{\max}$, with the error in the fourth decimal place in this case. The SMatPI results with up to $\Delta k_{\max} = 10$ are indistinguishable from those obtained through i-QuAPI calculations.

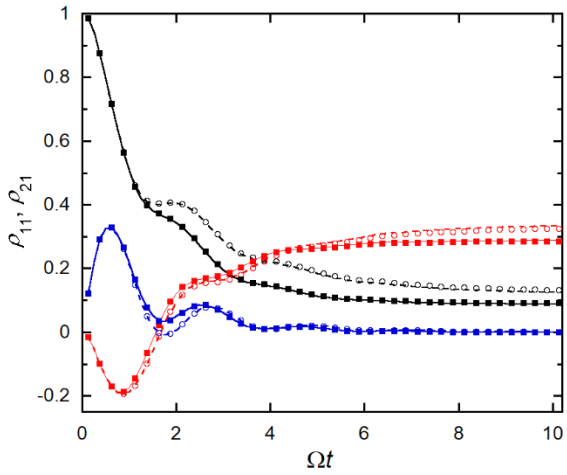

Fig. 5. SMatPI results showing the RDM elements for the asymmetric TLS with parameters described in the section IV. Dashed lines: $r_{\max} = \Delta k_{\max} = 5$. Hollow circles: $\Delta k_{\max} = 5$, $r_{\max} = 6$. Solid lines: $r_{\max} = \Delta k_{\max} = 10$. Solid markers: $\Delta k_{\max} = 10$, $r_{\max} = 11$. Black: diagonal element corresponding to initially populated state. Red and blue: real and imaginary parts of off-diagonal element $\tilde{\rho}_{21}$.

The last calculation examines the consequences of non-nearest neighbor coupling in a model system that involves $n = 11$ sites with, whose Hamiltonian is given by

$$\hat{H}_0 = -\hbar\Omega\sum_{i=1}^{n-1}\left(|\sigma_i\rangle\langle\sigma_{i+1}| + |\sigma_{i+1}\rangle\langle\sigma_i|\right) - V\sum_{i=1}^{n-2}\left(|\sigma_i\rangle\langle\sigma_{i+2}| + |\sigma_{i+2}\rangle\langle\sigma_i|\right), \tag{6.1}$$

where again $\Delta\sigma = 2$ is the outermost site distance, and

$$\sigma_1 = -1\,,\ \sigma_i = \sigma_1 + \frac{i-1}{n-1}\Delta\sigma\,. \tag{6.2}$$

In addition to nearest neighbor coupling, Eq. (6.1) contains next-nearest neighbor interactions. The 11-site system is coupled to a harmonic bath described by the spectral density given in Eq. (4.3) with parameters $\xi = 2$, and $\omega_c = 4\Omega$. The bath is initially at a temperature $\hbar\Omega\beta = 0.2$. The SMatPI calculations converged to 0.01 with $\Omega\Delta t = 0.1$ and $r_{\max} = \Delta k_{\max} = 5$, and the convergence was verified by increasing $r_{\max}$ and $\Delta k_{\max}$ to 6. The site populations reached their long-time equilibrium values around $\Omega t = 12$. To test the stability of the SMatPI method, the site populations were followed for 400 iteration steps, up to $\Omega t = 40$. The trace of the RDM remained equal to 1 within 8 decimal places over the entire propagation.

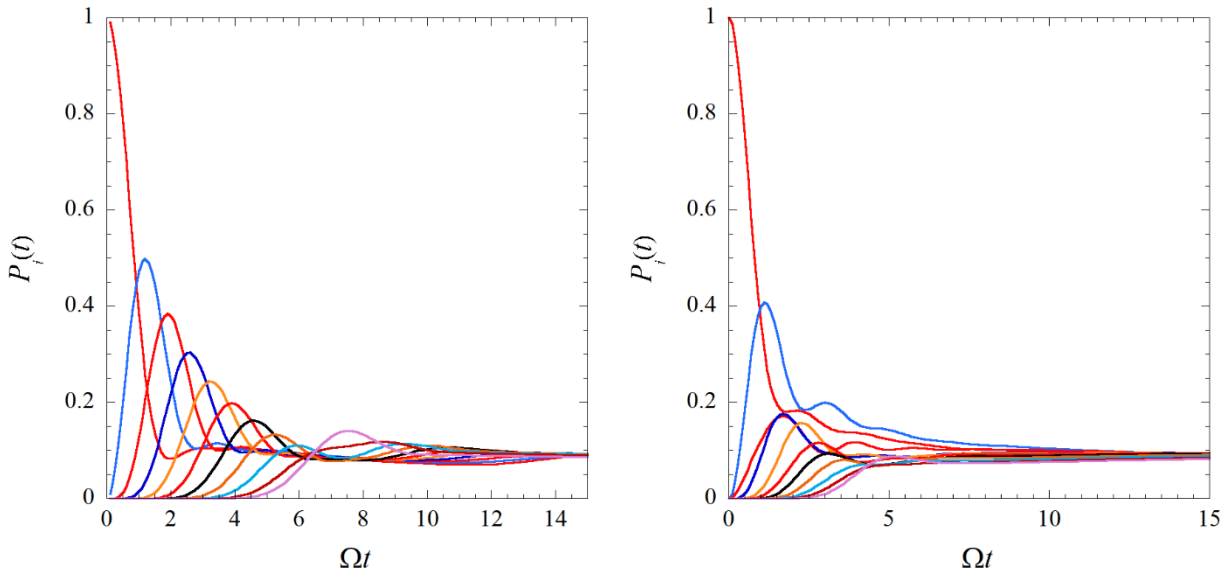

Fig. 6. Site populations for the 11-site Hamiltonian of Eq. (6.1) with parameters described in the text, computed via the SMatPI decomposition with $r_{\max} = \Delta k_{\max} = 6$. Initially only the first site is populated. The curve that starts at 1 is the population of site 1, while curves rising from zero correspond (from left to right) to the populations of sites 2-11. (a) Nearest neighbor interactions only. (b) Nearest and next-nearest neighbor interactions.

With these parameters, direct computation of the full forward-backward path sum for the same final time has 11^{802} terms. The i-QuAPI algorithm would require the storage of a tensor with $11^{10} \simeq 2.6\times10^{10}$ complex-valued amplitudes, and 400×11^{12} operations, and is impractical. By comparison, the SMatPI code involves storage of just ten 121×121 matrices (about 1.4×10^{5} elements), reducing the required array storage by a factor of 2×10^{5}. The most demanding step of the SMatPI calculation required a single sum of 11^{12} terms, i.e. the required CPU time is reduced by a factor of 400. These gains allow previously challenging calculations to be performed even on a laptop.

Figure 6a shows the results of SMatPI calculations with $V = 0$, for which the system contains only nearest neighbor couplings, while Figure 6b presents similar results for a Hamiltonian that includes next-nearest neighbor terms obtained with $V = -\frac{1}{2}\hbar\Omega$. In both cases, the site populations exhibit at long times a small spread about the value $1/n$, which is a consequence of the non-uniform contribution of the site coefficients to the system eigenstates. A comparison of the two figures reveals the role of next-nearest-neighbor couplings in the population dynamics. In the case of only nearest-neighbor terms, the populations approach their long time values with weak oscillatory components which are most clearly seen in sites near the edges. When the Hamiltonian includes next-nearest neighbor couplings, the decay of the initially populated and neighboring sites is more oscillatory, and population transfer to distant sites occurs faster.

VII. Concluding remarks

Iterative real-time path integral methods for non-Markovian quantum dissipative systems take advantage of the decay of temporal correlations to explicitly treat path segments that span only the bath-induced memory length of $\Delta k_{\max}$ time steps, leading to linear scaling with the number N of propagation steps. The resulting i-QuAPI algorithm[17, 18] requires the storage of a path array of size $n^{2\Delta k_{\max}}$, while propagation to the final time involves $N(n^2)^{\Delta k_{\max}+1}$ operations. Even though various array compression techniques (such as path filtering,[19-22] singular value tensor contraction[32] or the blip decomposition[28, 29]) can dramatically reduce the required storage, the contracted path array still exceeds (typically by several orders of magnitude) the size of the bare system's RDM, and often is prohibitively large.

The disentanglement of the path integral variables offers a powerful, numerically exact alternative to system-bath dynamics. Construction of the SMatPI matrices requires evaluation of a path sum that spans the entanglement length, which is practically equal to the bath-induced memory and thus involves (in the absence of filtering) $(n^2)^{\Delta k_{\max}+1}$ operations. The SMatPI decomposition eliminates the need for storing an array of $n^{2\Delta k_{\max}}$ system paths and the $N(n^2)^{\Delta k_{\max}+1}$ operations required for propagation to N time steps. The code required to evaluate the path sum is simple and straightforwardly parallelizable. Further, the disentanglement of the path integral variables – even *within* the memory length - offers new, valuable conceptual insights into the dynamics of quantum dissipative systems. The diagrammatic approach illustrated in Fig. 1 offers an intuitive justification of the SMatPI decomposition.

A number of techniques may be used to accelerate the calculation of the single $(n^2)^{\Delta k_{\max}+1}$-term sum required to obtain the SMatPI matrices. For example, path filtering[19-22] often leads to exponential reduction of the number of terms, and the blip decomposition[24] may be employed to eliminate the vast majority of forward-backward path pairs in regimes of incoherent dynamics. One could also resort to approximate procedures, such as the use of influence functional coarse graining techniques,[27, 30] for calculating the SMatPI matrices for the largest r values, which are the most costly but make small contribution.

By eliminating the need for storing and manipulating large arrays makes the SMatPI algorithm ideal for use with multistate systems, while retaining the rigorous, fully quantum mechanical real-time path integral approach. Because of their computational difficulty, numerically exact calculations on discrete systems have been limited to short-time dynamics or simplified system-bath models. The preliminary exploration of an 11-state model presented in section VI revealed interesting effects that warrant additional investigation. The SMatPI methodology can be used to provide definitive answers to questions related to the interplay between tunneling and thermal fluctuations in Caldeira-Leggett models,[5] to investigate quantum coherence in energy transfer through extended systems,[50, 51] and to quantify the role of competing pathways in bridge-mediated electron transfer.[52, 53] Further, by using traditional Cartesian reaction path[54] expansions of polyatomic potential surfaces and discretizing the system coordinate, one should be able to apply the SMatPI algorithm to the treatment of chemical reaction dynamics in polyatomic molecular systems. Some of these explorations are in progress in our group.

Acknowledgment

This material is based upon work supported by the National Science Foundation under Award CHE-1665281.

References

1. Meyer, H.-D.; Manthe, U.; Cederbaum, L. S., The multi-configurational time-dependent Hartree approach. *Chem. Phys. Lett.* **1990**, 165, 73-78.
2. White, S. R., Density matrix formulation for quantum renormalization groups. *Phys. Rev. Lett.* **1992**, 69, 2863.
3. Feynman, R. P., Space-time approach to non-relativistic quantum mechanics. *Rev. Mod. Phys.* **1948**, 20, 367-387.
4. Feynman, R. P.; Hibbs, A. R., *Quantum Mechanics and Path Integrals*. McGraw-Hill: New York, 1965.
5. Caldeira, A. O.; Leggett, A. J., Path integral approach to quantum Brownian motion. *Physica A* **1983**, 121, 587-616.
6. Leggett, A. J.; Chakravarty, S.; Dorsey, A. T.; Fisher, M. P. A.; Garg, A.; Zwerger, M., Dynamics of the dissipative two-state system. *Rev. Mod. Phys.* **1987**, 59, 1-85.
7. Weiss, U., *Quantum Dissipative Systems*. World Scientific: Singapore, 1993.
8. Feynman, R. P.; F. L. Vernon, J., The theory of a general quantum system interacting with a linear dissipative system. *Ann. Phys.* **1963**, 24, 118-173.
9. Ehrenfest, P., Bemerkung über die angenäherte Gültigkeit der klassischen Mechanik innerhalb der Quantenmechanik. *Z. Phys.* **1927**, 45, 455-457.
10. Lambert, R.; Makri, N., Quantum-classical path integral: Classical memory and weak quantum nonlocality. *J. Chem. Phys.* **2012**, 137, 22A552.
11. Lambert, R.; Makri, N., Quantum-classical path integral: Numerical formulation. *J. Chem. Phys.* **2012**, 137, 22A553.
12. Makri, N., Quantum-classical path integral: A rigorous approach to condensed phase dynamics. *International Journal of Quantum Chemistry* **2015**, 115, 1209-1214.

13. Walters, P. L.; Makri, N., Quantum-classical path integral simulation of the ferrocene-ferrocenium charge transfer in liquid hexane. *J. Phys. Chem. Lett.* **2015**, 6, 4959-4965.
14. Metropolis, N.; Rosenbluth, A. W.; Rosenbluth, M. N.; Teller, H.; Teller, E., Equation of state calculations by fast computing machines. *J. Chem. Phys.* **1953**, 21, 1087-1092.
15. Makri, N., Improved Feynman propagators on a grid and non-adiabatic corrections within the path integral framework. *Chem. Phys. Lett.* **1992**, 193, 435-444.
16. Topaler, M.; Makri, N., System-specific discrete variable representations for path integral calculations with quasi-adiabatic propagators. *Chem. Phys. Lett.* **1993**, 210, 448.
17. Makri, N.; Makarov, D. E., Tensor multiplication for iterative quantum time evolution of reduced density matrices. I. Theory. *J. Chem. Phys.* **1995**, 102, 4600-4610.
18. Makri, N.; Makarov, D. E., Tensor multiplication for iterative quantum time evolution of reduced density matrices. II. Numerical methodology. *J. Chem. Phys.* **1995**, 102, 4611-4618.
19. Sim, E.; Makri, N., Tensor propagator with weight-selected paths for quantum dissipative dynamics with long-memory kernels. *Chem. Phys. Lett.* **1996**, 249, 224-230.
20. Sim, E.; Makri, N., Filtered propagator functional for iterative dynamics of quantum dissipative systems. *Comp. Phys. Commun.* **1997**, 99, 335-354.
21. Sim, E., Quantum dynamics for a system coupled to slow baths: on-the-fly filtered propagator method. *J. Chem. Phys.* **2001**, 115, 4450-4456.
22. Lambert, R.; Makri, N., Memory path propagator matrix for long-time dissipative charge transport dynamics. *Mol. Phys.* **2012**, 110, 1967-1975.
23. Golosov, A. A.; Friesner, R. A.; Pechukas, P., Efficient memory equation algorithm for reduced dynamics in spin-boson models. *J. Chem. Phys.* **1999**, 110, 138-146.
24. Golosov, A. A.; Friesner, R. A.; Pechukas, P., Reduced dynamics in spin-boson models: A method for both slow and fast bath. *J. Chem. Phys.* **2000**, 112, 2095-2105.
25. Weiss, S.; Eckel, J.; Thorwart, M.; Egger, R., Iterative real-time path integral approach to nonequilibrium quantum transport. *Phys. Rev. B* **2008**, 77, 195316.
26. Dattani, N. S., Numerical Feynman integrals with physically inspired interpolation: Faster convergence and significant reduction of computational cost. *AIP Advances* **2012**, 2, 012121.
27. Makri, N., Path integral renormalization for quantum dissipative dynamics with multiple timescales. *Mol. Phys.* **2012**, 110, 1001-1007.
28. Makri, N., Blip decomposition of the path integral: Exponential acceleration of real-time calculations for quantum dissipative systems. *J. Chem. Phys.* **2014**, 141, 134117.
29. Makri, N., Iterative blip-summed path integral for quantum dynamics in strongly dissipative environments. *J. Chem. Phys.* **2017**, 146, 134101.
30. Richter, M.; Fingerhut, B. P., Coarse-grained representation of the quasiadiabatic propagator path integral for the treatment of non-Markovian long-time bath memory. *J. Chem. Phys.* **2017**, 146, 214101.
31. Nalbach, P.; Palm, P., Quasi-adiabatic path integral approach for quantum systems under the influence of multiple non-commuting fluctuations. *J. Chem. Phys.* **2018**, 149, 214103.
32. Strathearn, A.; Kirton, P.; Kilda, D.; Keeling, J.; Lovett, B. W., Efficient non-Markovian quantum dynamics using time-evolving matrix product operators. *Nature Communications* **2018**, 9, 3322.
33. Segal, D.; Reichman, D. R.; Millis, A. J., Nonequilibrium quantum dissipation in spin-fermion systems. *Phys. Rev. B* **2007**, 76, 195316.
34. Segal, D.; Millis, A. J.; Reichman, D. R., Numerically exact path integral simulation of nonequilibrium quantum transport and dissipation. *Phys. Rev. B* **2010**, 82, 205323.
35. Makri, N., Iterative evaluation of the path integral for a system coupled to an anharmonic bath. *J. Chem. Phys.* **1999**, 111, 6164-6167.
36. Makri, N., Modular path integral: Quantum dynamics via sequential necklace linking. *J. Chem. Phys.* **2018**, 148, 101101.
37. Makri, N., Modular path integral methodology for real-time quantum dynamics. *J. Chem. Phys.* **2018**, 149, 214108.

38. Makri, N., Numerical path integral techniques for long-time quantum dynamics of dissipative systems. *J. Math. Phys.* **1995**, 36, 2430-2456.
39. Makri, N., Small matrix disentanglement of the path integral: overcoming the exponential tensor scaling with memory length. *J. Chem. Phys.* **2020**, 152, 041104.
40. Trotter, M. F., On the product of semi-groups of operators. *Proc. Am. Math. Soc.* **1959**, 10, 545-551.
41. Allen, T. C.; Walters, P. L.; Makri, N., Direct computation of influence functional coefficients from numerical correlation functions. *J. Chem. Theory and Comput.* **2016**, 12, 4169-4177.
42. Nalbach, P.; Thorwart, M., Ultraslow quantum dynamics in a sub-Ohmic heat bath. *Phys. Rev. B* **2010**, 81, 054308.
43. Walters, P. L.; Banerjee, T.; Makri, N., On iterative path integral calculations for a system interacting with a shifted dissipative bath. *J. Chem. Phys.* **2015**, 143, 074112.
44. Nalbach, P.; Eckel, J.; Thorwart, M., Quantum coherent biomolecular energy transfer with spatially correlated fluctuations. *New Journal of Physics* **2010**, 12, 065043.
45. Makarov, D. E.; Makri, N., Stochastic resonance and nonlinear response in double quantum well structures. *Phys. Rev. B* **1995**, 52, R2257-2260.
46. Shao, J.; Makri, N., Iterative path integral calculation of quantum correlation functions for dissipative systems. *Chem. Phys.* **2001**, 268, 1-10.
47. Shao, J.; Makri, N., Iterative path integral formulation of equilibrium correlation functions for quantum dissipative systems. *J. Chem. Phys.* **2002**, 116, 507-514.
48. Nakajima, S., On quantum theory of transport phenomena. *Prog. Theor. Phys* **1958**, 20, 948.
49. Cerrillo, X.; Cao, J., Non-Markovian Dynamical Maps: Numerical Processing of Open Quantum Trajectories. *Phys. Rev. Lett.* **2014**, 112, 110401.
50. Mujica, V.; Nitzan, A.; Mao, Y.; Davis, W.; Kemp, M.; Roitberg, A.; Ratner, M. A., Electron transfer in molecules and molecular wires: Geometry dependence, coherent transfer, and control. *Adv. Chem. Phys.* **1999**, 107, 403-439.
51. May, V.; Kuhn, O., *Theory of charge and energy transfer in molecular systems*. Wiley: 1999.
52. Onuchic, J. N.; Beratan, D. N.; Winkler, J. R.; Gray, H. B., Pathway analysis of protein electron transfer reactions. *Ann. Rev. Biophys. Biom. Struc.* **1992**, 21, 349.
53. Beratan, D. N.; Skourtis, S. S.; Balabin, I. A.; Balaeff, A.; Keinan, S.; Venkatramani, R.; Xiao, D., Steering electrons on moving pathways. *Acc Chem Res.* **2009**, 42, 1669–1678.
54. Ruf, B. A.; Miller, W. H., A new (Cartesian) reaction path model for dynamics in polyatomic systems, with application to H atom transfer in malonaldehyde. *J. Chem. Soc., Faraday Trans. 2* **1988**, 84, 1523-1534.

TOC figure:

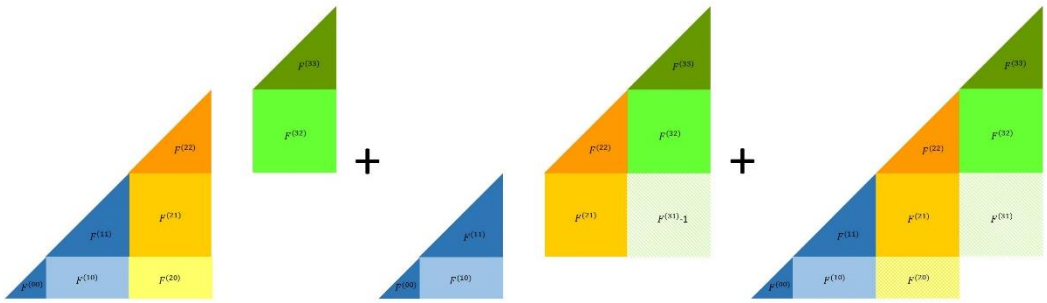
F(33)
F(32)
F(22)
F(21)
F(11)
F(10)
F(20)
F(00)
+
F(33)
F(32)
F(11)
F(10)
F(00)
+
F(33)
F(22)
F(32)
F(21)
F(31)-1
+
F(33)
F(22)
F(32)
F(11)
F(21)
F(31)
F(10)
F(70)
F(00)